International Journal of Pharmaceutics 388 (2010) 101–106

Contents lists available at ScienceDirect

International Journal of Pharmaceutics

journal homepage: www.elsevier.com/locate/ijpharm

Modelling of porosity and waterfronts in cellulosic pellets for understanding drug release behavior

Ana Gomez-Carracedo, Ramon Martinez-Pacheco, Angel Concheiro, Jose Luis Gomez-Amoza*

Departamento de Farmacia y Tecnologia Farmaceutica, Universidad de Santiago de Compostela, Santiago de Compostela 15782, Spain

ARTICLE INFO

Article history:
Received 30 July 2009
Received in revised form
14 December 2009
Accepted 19 December 2009
Available online 28 December 2009

Keywords:
Network modelling
Pore-Cor™ software
Extrusion–spheronization
Pellet microstructure
Drug delivery
Water uptake

ABSTRACT

The microstructure of cellulose microcrystalline-Carbopol® pellets, prepared under different drying conditions (oven-dried or freeze-dried), was experimentally characterized using mercury intrusion porosimetry and then computationally modelled using Pore-Cor™ software. Connectivity (mean number of throats per pore), pore skew (σ), throat skew (q) and correlation level were estimated and simultaneously optimized from the mercury intrusion porosimetry cumulative curves using the Boltzmann-annealed simplex algorithm. Unit cells with percolation properties close to the real ones were generated. Water penetration rate in the simulated structures was also modelled using Pore-Cor™ and the waterfront position was calculated using the Bosanquet equation. A close correlation was found between the simulated water flow rate in the unit cell and the experimental theophylline first-order release rate constant. Thus, modelling of network microstructure and waterfronts appears as an useful tool for predicting drug release rate from matrix pellets.

1. Introduction

The microstructure of pellets depends on starting materials, processing approach and fabrication conditions, and determines to a large extent their mechanical features and their performance as drug delivery systems (Gomez-Carracedo et al., 2007; Balaxi et al., 2009a,b). As for other porous solids, pellet microstructure is quite complex with pores of diverse shapes and sizes, which makes the study of drug transport through the network difficult (Armatas and Pomonis, 2004). Mercury intrusion porosimetry can inform about total porosity, pore size distribution, pore connectivity and tortuousness (Laudone et al., 2008; Gomez-Carracedo et al., 2009). This information is the basis for predicting the topology of porous structures using geometric models of various complexities, such as random-loose packing of spheres that are overlapped to achieve a given void fraction (Zalc et al., 2003, 2004) or two- and three-dimensional lattices of complex pore shapes (Kloubek, 1994) or cylindrical- or cubic-shaped pores (Wood and Gladden, 2002a,b). Based on the latter approach, Pore-Cor™ software is particularly useful for modelling the porous structure of most materials (e.g., soils, sandstones, compacted mineral blocks, catalysts, paper coatings or pharmaceutical tablets) since makes the prediction of the hydraulic conductivity, the liquid permeation or the water retention in porous materials possible (Ridgway et al., 1997; Johnson et al., 2003; Bodurtha et al., 2005; Laudone et al., 2005, 2007; Schoelkopf et al., 2000b; Holtham et al., 2007). Pore-Cor™ enables the generation of a three-dimensional void structure that has the same percolation characteristics as those of the material experimentally characterized by mercury intrusion porosimetry. Roughly, the modelling assumes that the material consists in interconnected unit cells of 1000 pores (of arbitrary cubic shape) arranged in a regular three-dimensional $10 \times 10 \times 10$ array and connected by up to 3000 throats (of arbitrary cylindrical shape). The number of throats depends on the connectivity of the pores and ranges from 1, when there is one throat per pore, to 6 if each pore is connected to 6 neighbor pores by throats. In each unit cell, the centers of the pores are equidistant each other; the distance being the pore range spacing Q. Thus, each unit cell is a cube-like structure possessing 10 Q length sides (Ridgway et al., 2006). Connecting throats are generated to have sizes between the greatest and the lowest pore diameters (i.e., between d_{max} and d_{min}) experimentally obtained by mercury intrusion porosimetry. The throat size distribution fits to log-normal distribution with a throat skew, q, ranging from −50 (distribution skewed to d_{min}) to 50 (skewed to d_{max}). Each cubic pore has a size equals to the size of the greatest throat connect to it multiplied by a pore skew, σ, which has values ranging from 1 to d_{max}/d_{min} (Johnson et al., 2003). Throats and pores are arranged in the three-dimensional $10 \times 10 \times 10$ array according to the value of the *correlation level*. This parameter has values between 0 (random spatial arrangement) and 1 (arrangement of throats and pores as a function of their sizes)

* Corresponding author. Tel.: +34 981563100; fax: +34 981547148.
E-mail address: joseluis.gomez.amoza@usc.es (J.L. Gomez-Amoza).

0378-5173/$ – see front matter © 2009 Elsevier B.V. All rights reserved.
doi:10.1016/j.ijpharm.2009.12.038

(Peat et al., 2000). The modelling begins placing the throats in the unit cell. Then, 1000 pores are placed in such a way that each one is connected to neighbor pores by at least one throat. Increasing or diminishing the value of *Q*, i.e., changing the size of the unit cell, the throats are enlarged or shortened in order to bring the porosity close to its experimental value. Pore-Cor™ software enables the simulation of the mercury intrusion process in the unit cell and compares the simulated pore size *vs*. volume curve to that experimentally obtained (in both cases normalized porosities are used). The goodness of the fitting is indicated by the distance parameter, *f*, which gives the mean distance between the experimental intrusion curve data points and the closets data points of the simulated intrusion curve. Since the *X*-axis of those plots is logarithmic and the *Y*-axis shows normalized porosity data, *f* is also normalized and adimensional. Values of *f* close to or smaller than 1 indicate that the simulated model truly represents the behavior of the real material (Johnson et al., 2003).

Although still few, some papers have shown the potential of using Pore-Cor™ network simulator in the pharmaceutical field with the aim of gaining insight into the incidence of formulation variables on the microstructural properties of pellets and tablets (Ridgway et al., 1997; Gane et al., 2006). However, to the best of our knowledge, no attempts to correlate parameters coming from Pore-Cor™ modelling with the drug release behavior of solid dosage forms have been made yet. The aim of this work was to model the microstructure of matrix pellets, to elucidate the incidence of composition and drying procedure on the microstructure, and to correlate drug dissolution rate with simulated microstructure-dependent parameters.

2. Materials and methods

2.1. Materials

Theophylline was from Sigma–Aldrich (Spain), Carbopol® 974P from Lubrizol Corp. (Ohio USA), microcrystalline cellulose (MCC) Avicel® PH101 from FMC (New Jersey USA), lactose anhydrous from Fagron Ibérica (Spain) and dicalcium phosphate dihydrate (DCP) from Merck (Germany).

2.2. Preparation of pellets

Pellets were prepared by extrusion–spheronization as previously reported (Gomez-Carracedo et al., 2007, 2008, 2009). Pellets designed by code L had 20% theophylline, 48% Carbopol® 974P, 24% MCC, and 8% lactose. Pellets designed by code F had the same composition as above but replacing lactose by DCP. The pellets were dried using different techniques: (a) hot air oven at 40 °C for 24 h (OD) (batches L1 and F1); (b) freeze-drying after fast freezing in liquid nitrogen (FD Fast) (batches L2 and F2); or (c) freeze-drying after slow freezing at −30 °C for 24 h (FD Slow) (batches L3 and F3) (Table 1).

2.3. Theophylline release profiles

Drug release profiles of pellets (250 mg) were obtained, in sextuplicate, using a USP24 type II apparatus (Turu Grau, Spain) at 50 rpm and 37 °C, in 900 ml of water. Drug concentration was determined spectrophotometrically at 271 nm (Agilent 8453, Germany). Drug release profiles were fitted by non-linear regression (GraphPad Prism v. 3.02, GraphPad Software Inc., San Diego, CA, USA) to a first-order model, namely $D = 1 - e^{-Kt}$, where D represents theophylline dose fraction release at time t and K is the dissolution rate constant (Gomez-Carracedo et al., 2008).

2.4. Mercury intrusion porosimetry and pore modelling

The pellets were analyzed in triplicate using a Micromeritics 9305 pore sizer (Norcross GA, USA) fitted with a 3-ml powder penetrometer (0.004–172.4 MPa, 30 s for equilibration after each intrusion step). Raw intrusion values were corrected using PoreComp™ 6.11 software (Environmental and Fluid Modelling Group, University of Plymouth, UK), which takes into account the mercury compression, the penetrometer expansion, and the compressibility of the sample (Gane et al., 1995). Pore size data were fitted to bimodal log-normal distributions and the subpopulations of lower mode were assigned to the intrapellet void spaces (Gomez-Carracedo et al., 2009). This lower size population was used for modelling the porous structure of pellets as connected unit cells using Pore-Cor™ 6.11 software (Environmental and Fluid Modelling Group, University of Plymouth, UK). The connectivity (mean number of throats per pore), the pore skew (σ) and the throat skew (q) and the correlation level (between 0, random structure, and 1, organization in the unit cell) were estimated and simultaneously optimized from the mercury intrusion porosimetry cumulative curves using the Boltzmann-annealed simplex algorithm (Johnson et al., 2003). In addition to the restrictions in the values of these four parameters, explained in the introduction, we have also taken into account that: (i) the resulting structure of the unit cell should fit to the experimental porosity avoiding the overlapping of pores; (ii) there is not closed pores; and (iii) the geometric parameters are actually or potentially verifiable by experimental data (Johnson et al., 2003). In such a way, the four parameters should enable the generation of unit cells with percolation properties close to the real ones.

The water penetration rate in the simulated structures was modelled using Pore-Cor™ and the waterfront position was calculated using the Bosanquet equation (Schoelkopf et al., 2000b):

$$x_2^2 - x_1^2 = \left(\frac{2B}{A}\right)\left(t - \left(\frac{1}{A}\right)(1 - \exp(-At))\right),$$

$$\text{with } A = \frac{8\eta}{\rho r^2} \text{ and } B = \frac{P_e r + 2\gamma\cos\theta}{r\rho}$$

where x_1 and x_2 are the positions of the liquid front at the beginning and at time t, respectively, P_e the external pressure applied at the entrance of pores and throats, η the water dynamic viscosity (0.001 Pa s), ρ the water density (998 kg m^{-3}), γ the water surface tension (72.75 × 10^{-3} N m^{-1}), θ the solid–water contact angle (50°), and r the pore radius. Water was assumed to enter from the upper face of the unit cell and that the flow occurred in the $-z$, $\pm x$ and $\pm y$ directions. Once the position of the liquid front was estimated at several times, the volumes of the void spaces of the unit cells filled by the fluid were estimated. The plot of filled volume (v) *vs*. time (t) was fitted to the power-law equation $v = mt^n$, in which m and n are the scale factor and the shape factor, respectively.

3. Results and discussion

3.1. Modelling of the microporous structure

Cumulative pore size curves obtained by mercury intrusion porosimetry and the modelled intragranular void spaces (using Pore-Cor™) are shown in Fig. 1. The distance parameter, *f*, was in all cases below 1.15, which means a good fitting (Johnson et al., 2003). Fig. 1B summarizes the estimated values for the parameters optimized by the modelling software and Fig. 2 shows the 3-D structure of the unit cell of each batch of pellets. It is clear that the complexity of the void network of a natural sample can be hardly generated using the relatively simple geometry of the Pore-Cor unit cell. Frequently, the size of the unit cells is smaller than that of

Table 1
Formulation variables of theophylline pellets prepared with MCC and Carbopol® 974P by extrusion–spheronization, mercury intrusion data, Pore-Cor™ modelling parameters, and theophylline first-order release rate constant.

Property	Pellets code					
	L1	L2	L3	F1	F2	F3
Co-filler	Lactose	Lactose	Lactose	DCP	DCP	DCP
Drying[a]	OD	FD Fast	FD Slow	OD	FD Fast	FD Slow
Porous volume,[b] $cm^3\ g^{-1}$	0.016 (0.003)	0.183 (0.009)	0.092 (0.007)	0.017 (0.002)	0.282 (0.011)	0.126 (0.010)
Mean throat size,[c] μm	0.012 (0.006)	0.487 (0.010)	0.616 (0.018)	0.010 (0.007)	0.481 (0.020)	0.535 (0.010)
Mean pore size,[c] μm	0.024 (0.004)	2.800 (0.098)	3.252 (0.087)	0.029 (0.004)	3.565 (0.102)	3.606 (0.078)
n[b]	0.342 (0.015)	0.451 (0.029)	0.400 (0.020)	0.315 (0.021)	0.482 (0.016)	0.414 (0.025)
K,[d] h^{-1}	7.19 (0.38)	19.89 (1.06)	14.25 (0.54)	6.63 (0.36)	24.22 (0.67)	16.19 (1.18)

[a] OD, oven-drying; FD fast, freeze-drying after freezing by immersion in liquid nitrogen (−196 °C); FD slow, freeze-drying after freezing at −30 °C.
[b] Mean value and standard deviation (three replicates).
[c] Mean and standard deviation of the geometric means of three distributions.
[d] Mean and standard deviation of 6 replicates.

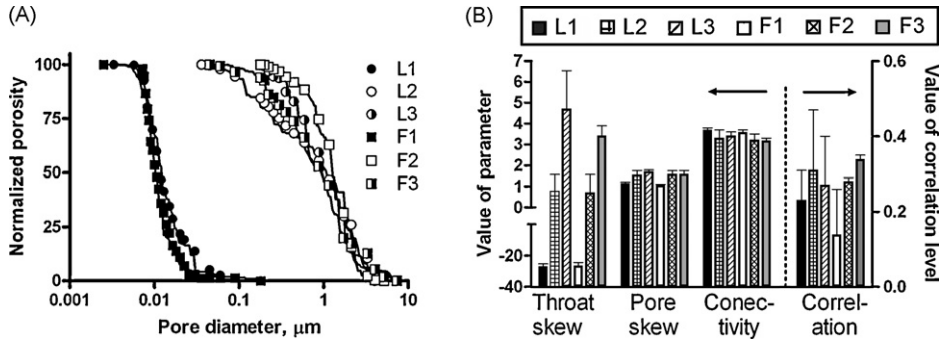

Fig. 1. (A) Pore-Cor™ simulation fitting of the cumulative pore size distributions of pellets (symbols: experimental data; lines: predicted values). (B) Mean values and standard deviations of the four parameters estimated using Pore-Cor™ software.

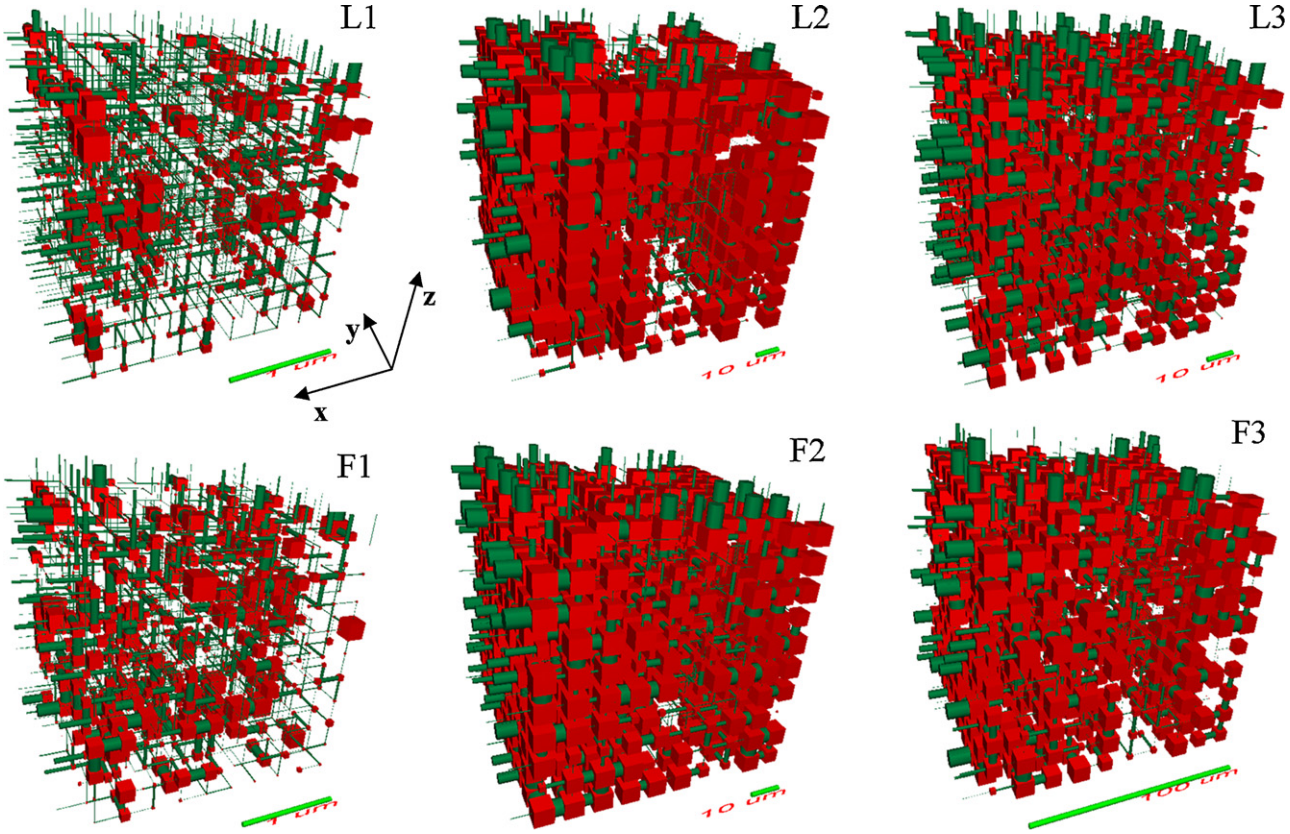

Fig. 2. Unit cells of pellets as modelled from mercury intrusion porosimetry data using Pore-Cor™ software (green color indicates the throats, red color the pores, and the white color the solid material). (For interpretation of the references to color in this figure legend, the reader is referred to the web version of the article.)

the representative elementary volume of the material (Schoelkopf et al., 2004). However, the combination of cubic pores with cylindrical throats (shape also assumed in intrusion mercury analysis; Perez Bernal and Bello, 2001) provides enough versatility to closely adjust the simulated percolation curve to the experimental mercury intrusion curve. Furthermore, the percolation features do not depend on Q and, consequently, the size of the unit cell (Schoelkopf et al., 2004).

The ANOVA of correlation and connectivity values (Fig. 1B) (GraphPad Prism v.5.00, GraphPad Software Inc., San Diego, CA) indicated that the pellet formulations are not different ($F = 1.40$ for correlation and $F = 2.48$ for connectivity, with 5 and 12 d.f.). Therefore, the drying process and the replacement of lactose by phosphate do not change the connectivity and the spatial arrangement of the pores. Oppositely, the throat skew and the pore skew were significantly different ($F = 284.30$ and $F = 10.64$, respectively, with 5 and 12 d.f.; $\alpha < 0.05$). The Newman–Keuls multiple comparison test revealed differences between oven-dried pellets (batches L1 and F1, with lower throat skew and pore skew) and freeze-dried pellets (batches L2, L3, F2 and F3). Geometric mean of pore sizes (in the d_{min} to d_{max} interval) of oven-dried pellets was 0.024 μm for L1 and 0.021 μm for F1, while the geometric mean of throat sizes was remarkably lower, 0.012 and 0.010 μm respectively (Table 1). Such a difference explains that throat skew values were clearly below 1 (Matthews et al., 2006). These findings confirm that oven-drying causes significant shrinking of the spheronized masses (Kleinebudde, 1994; Sousa et al., 1996; Vervaet et al., 1995) while the freezing before freeze-drying prevents the shrinking, particularly if the pellets are frozen by immersion in liquid nitrogen. Thus, freeze-dried pellets have greater void spaces than oven-dried pellets (Table 1). Fast freezing leads to small but numerous ice nuclei. Slow freezing promotes the formation of less ice nuclei that grow up and that, after water sublimation, lead to greater pores (Gomez-Carracedo et al., 2007; Balaxi et al., 2009b). In fact, the mean throat and the mean pore diameter were greater for the slowly frozen pellets (L3: 0.616 and 3.252 μm and F3: 0.535 and 3.606 μm) than for the rapidly frozen ones (L2: 0.487 and 2.800 μm and F2: 0.481 and 3.565 μm) (Table 1). Thus, modelling reveals that the drying process is a key factor for controlling the size of pores and throats, but it does not modify the connectivity and the spatial arrangement of pores.

3.2. Modelling of the water uptake

Drug release requires that the release medium penetrates into the pellet. Water uptake was modelled using the Bosanquet equation which has the advantage, compared to the Washburn equation, of taking into account the inertial effects. This aspect is particularly relevant when short time intervals are considered (Ridgway et al., 2002). Pore-Cor™ simulator assumes that the liquid enters into each throat in the form of a monolithic block of fluid (Schoelkopf et al., 2000b). Once a throat is full, the excess of liquid leaves this throat (the flow rate is calculated) and fills the adjacent pore. Each pore can receive liquid from various throats (depending of the connectivity of the system) and, once completely full, the liquid moves towards the throats connected to the pore that are not filled yet. Thus, the cubic pores behave as fluid reservoirs for the wetting of the throats. Such a simplified view of the wetting process does not require to take into account complex phenomena such as side-wall wetting, fingering, or groove and wedge capillarity (Schoelkof et

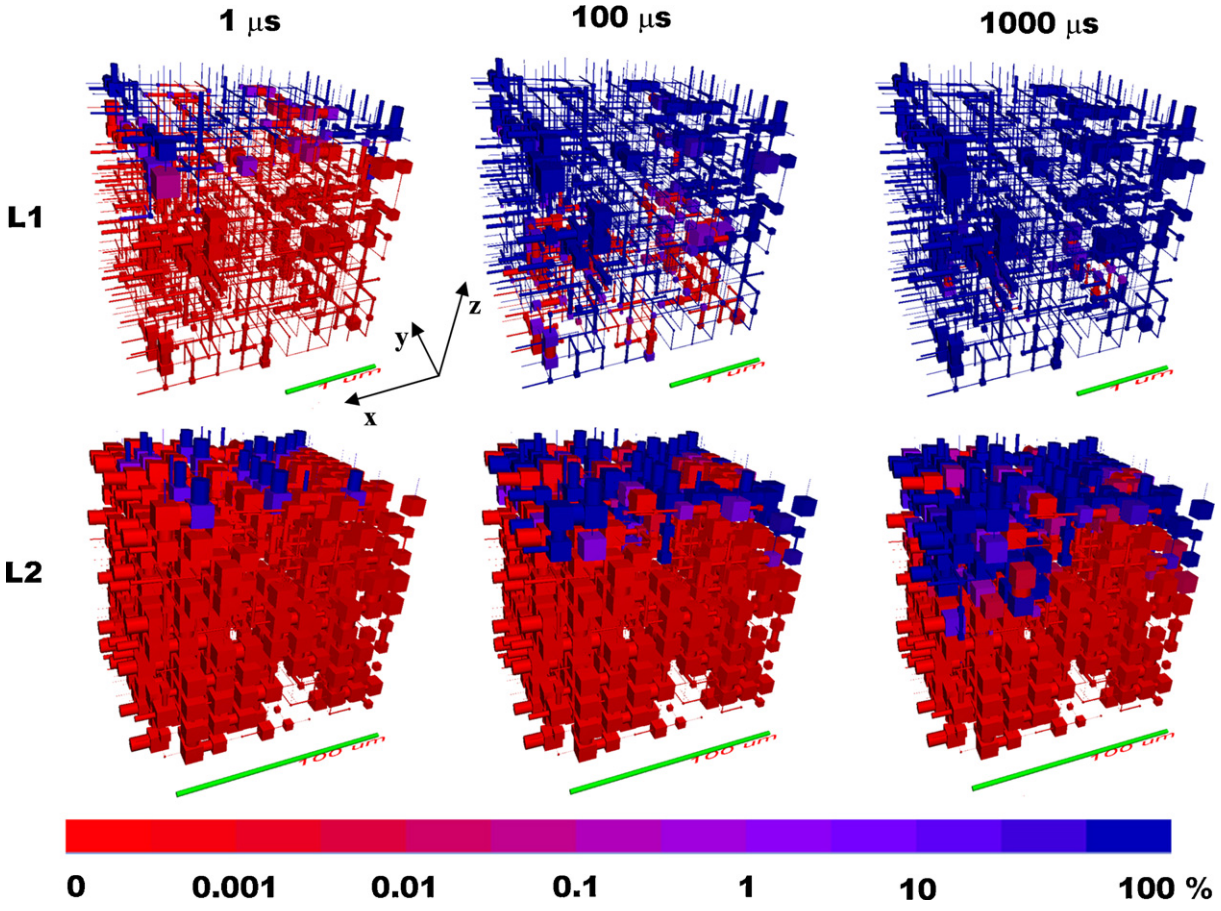

Fig. 3. Unit cells of L1 and L2 pellets showing water entrance (blue) in the voids (red) after 1, 100 and 1000 μs. (For interpretation of the references to color in this figure legend, the reader is referred to the web version of the article.)

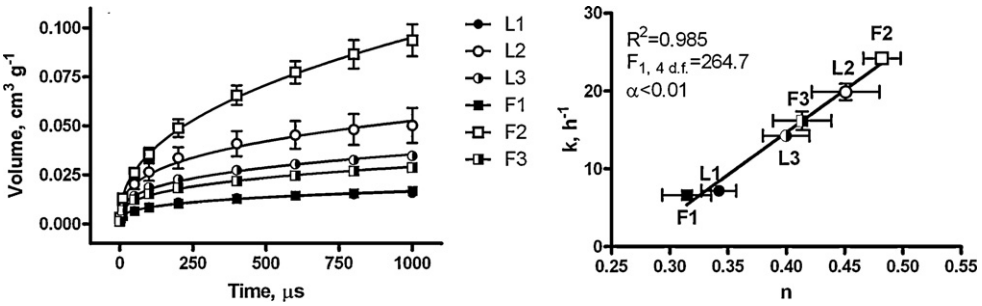

Fig. 4. (A) Water penetration profiles simulated using Pore-Cor software (symbols) and fitting to the power-law equation (lines); (B) linear correlation between the power-law exponent *n* and the experimental theophylline release rate constants.

al., 2004). Fig. 3 shows the position of the liquid front in the modelled microstructure of L1 and L2 pellets after 1, 100 and 1000 μs. A fast water uptake can be observed; 1 ms being enough to complete the water filling of the unit cell simulated for L1 pellets. In such a short period of time, the modelling of the water uptake enables to know how the water enters into the intrapellet void space, before the swelling or the dissolution of components could alter the pellet microstructure.

The plots of the mean volumes of the void spaces filled with water *vs.* time (Fig. 4A) revealed that oven-dried pellets (batches L1 and F1) finish water uptake in a shorter time but the total volume is lower than that uptaken by freeze-dried pellets (particularly by batches L2 and F2). The differences in water uptake are related to total porosity and the throat size, since the connectivity and the spatial arrangement of the pores are similar for all unit cells generated for the pellets of the present study.

The porosity determines the volume of liquid taken up, since no close pores were considered in the modelling. This explains the greater volume of water that can enter into the unit cells of freeze-dried pellets. On the other hand, the throat size determines the flow rate, since the cubic pores only act as reservoirs. Gane et al. (2000) and Schoelkopf et al. (2000a) have shown that, at the very beginning of the water entrance through pores greater than 0.1 μm, the flow is slowed due to the mass which has to be accelerated according to the Newton's law. This phenomenon leads to water uptake profiles that depend on the square-root of time (Ridgway and Gane, 2002). Such a behavior is not observed when the throats are smaller than 0.1 μm, rendering greater flow rates.

Oven-dried pellets with mean throat sizes below 0.1 μm (Table 1) rapidly take the water up but, due to their low porosity, the total volume is small. Their water uptake profile is not dependent on the square-root of time (power-law fitting, $n = 0.30–0.35$, Table 1). By contrast, the mean throat sizes of freeze-dried pellets greater than 0.1 μm explain the delayed water uptake and its dependence on the square-root of time (Table 1). The freeze-dried pellets can host more water due to their greater porosity, compared to the oven-dried ones.

3.3. Theophylline release profiles

Theophylline dissolution profiles were experimentally obtained and fitted to first-order kinetics (Gomez-Carracedo et al., 2008). The release from any pellet formulation was completed in 30 min. Release rate constants (K) were in the 7–23 h^{-1} range (Table 1). A close relationship between the power-law exponent, *n,* corresponding to the water uptake (simulated using Pore-Cor™ software) and the experimental drug release rate constants was observed (Fig. 4B). Although assuming differences in temporal scale when comparing simulated water uptake with experimental theophylline release, the simulated amount and rate of water uptake enable to relate formulation-dependent microstructural features and drug release rate and even to predict for a certain range of compositions how the delivery will take place.

4. Conclusions

Modelling of pellet microstructure is a valuable tool for gaining insight into the effect of the preparation variables on the size and distribution of the pores. Oven-dried pellets resulted in lower throat skew and pore skew than freeze-dried pellets. Such differences remarkably determined the entrance of water in the pellet matrix. The close relationship found between the simulated water flow rate and the experimental drug release rate highlights the interest of the modelling as a tool for predicting drug release behavior from solid dosage forms, just starting from mercury intrusion data and applying Pore-Cor™ network simulator.

Acknowledgements

Work supported by FEDER and Xunta de Galicia (DOG 31/08/2007, 07CSA006203PR). Dr. C. Alvarez-Lorenzo is acknowledged for her valuable help and suggestions.

References

Armatas, G.S., Pomonis, P.J., 2004. A Monte Carlo pore network for the simulation of porous characteristics of functionalized silica: pore size distribution, connectivity distribution and mean tortuosities. Chem. Eng. Sci. 59, 5735–5749.
Balaxi, M., Nikolakakis, I., Kachrimanis, K., Malamataris, S., 2009a. Combined effects of wetting, drying, and microcrystalline cellulose type on the mechanical strength and disintegration of pellets. J. Pharm. Sci. 98, 676–689.
Balaxi, M., Nikolakakis, I., Malamataris, S., 2009b. Preparation of porous microcrystalline cellulose pellets by freeze-drying: effects of wetting liquid and initial freezing conditions. J. Pharm. Sci., 10.1002/jps.
Bodurtha, P., Matthews, G.P., Kettle, J.P., Roy, I.M., 2005. Influence of anisotropy on the dynamic wetting and permeation of paper coatings. J. Colloid Interface Sci. 283, 171–189.
Gane, P.A.C., Kettle, J.P., Matthews, G.P., Ridgway, C.J., 1995. Void space structure of compressible polymer spheres and consolidated calcium carbonate paper-coating formulations. Ind. Eng. Chem. Res. 35, 1753–1764.
Gane, P.A.C., Ridgway, C.J., Barcelo, E., 2006. Analysis of pore structure enables improved tablet delivery systems. Powder Technol. 169, 77–83.
Gane, P.A.C., Schoelkopf, J., Spielmann, D.C., Matthews, G.P., 2000. Fluid transport into porous coating structures: some novel findings. Tappi J. 83, 77–78.
Gomez-Carracedo, A., Alvarez-Lorenzo, C., Coca, R., Martinez-Pacheco, R., Concheiro, A., Gomez-Amoza, J.L., 2009. Fractal analysis of SEM images and mercury intrusion porosimetry data for the microstructural characterization of microcrystal line cellulose-based pellets. Acta Mater. 57, 295–303.
Gomez-Carracedo, A., Souto, C., Martinez-Pacheco, R., Concheiro, A., Gomez-Amoza, J.L., 2008. Incidence of drying on microstructure and drug release profiles from tablets of MCC-lactose-Carbopol and MCC-dicalcium phosphate-Carbopol pellets. Eur. J. Pharm. Biopharm. 69, 675–685.
Gomez-Carracedo, A., Souto, C., Martinez-Pacheco, R., Concheiro, A., Gomez-Amoza, J.L., 2007. Microstructural and drug release properties of oven-dried and of slowly or fast frozen freeze-dried MCC-Carbopol pellets. Eur. J. Pharm. Biopharm. 67, 236–245.
Holtham, D.A.L., Matthews, G.P., Scholefield, D.S., 2007. Measurement and simulation of void structure and hydraulic changes caused by root-induced soil structuring under white clover compared to ryegrass. Geoderma 142, 142–151.

Johnson, A., Roy, I.M., Matthews, G.P., Patel, D., 2003. An improved simulation of void structure, water retention and hydraulic conductivity in soil with the Pore-Cor three-dimensional network. Eur. J. Soil Sci. 54, 477–489.

Kleinebudde, P., 1994. Shrinking and swelling properties of pellets containing microcrystalline cellulose and low substituted hydroxypropylcellulose 2. Shrinking properties. Int. J. Pharm. 109, 209–219.

Kloubek, J., 1994. Investigation of porous structures using mercury reintrusion and retention. J. Colloid Interface Sci. 163, 10–18.

Laudone, G.M., Matthews, G.P., Gane, P.A.C., Matthews, A.G., Ridgway, C.J., Schoelkopf, J.S.A., Huggett, S.A., 2007. Estimation of structural element sizes in sand and compacted blocks of ground calcium carbonate using a void network model. Transp. Porous Med. 66, 403–419.

Laudone, G.M., Matthews, G.P., Gane, P.A.C., 2008. Modelling diffusion from simulated porous structures. Chem. Eng. Sci. 63, 1987–1996.

Laudone, G.M., Matthews, G.P., Gane, P.A.C., Ridgway, C.J., Schoelkopf, J., 2005. Estimation of the effective particle sizes within a paper coating layer using a void network model. Chem. Eng. Sci. 60, 6795–6802.

Peat, D.M.W., Matthews, G.P., Worsfold, P.J., Jarvis, S.C., 2000. Simulation of water retention and hydraulic conductivity in soil using three-dimensional network. Eur. J. Soil Sci. 51, 65–79.

Perez Bernal, J.L., Bello, M.A., 2001. Fractal geometry and mercury porosimetry. Comparison and application of proposed models on building stones. App. Surf. Sci. 185, 99–107.

Ridgway, C.J., Gane, P.A.C., 2002. Dynamic absorption into simulated structures. Colloids Surf. A 206, 217–239.

Ridgway, C.J., Gane, P.A.C., El Abd, A.E., Czachor, A., 2006. Water absorption into construction materials: comparison of neutron radiography data with network absorption models. Transp. Porous Med. 63, 503–525.

Ridgway, C.J., Gane, P.A.C., Schoelkopf, J., 2002. Effect of capillary element aspect ratio on the dynamic imbibition within porous networks. J. Colloid Interface Sci. 252, 373–382.

Ridgway, C.J., Ridgway, K., Matthews, G.P., 1997. Modelling of the void space of tablets compacted over a range of pressures. J. Pharm. Pharmacol. 49, 377–383.

Schoelkopf, J., Gane, P.A.C., Ridgway, C., 2004. A comparison of the various liquid interactions radii derived from experiment and network modeling of porous pigmented structures. Colloids Surf. A 251, 149–159.

Schoelkopf, J., Gane, P.A.C., Ridgway, C.J., Matthews, G.P., 2000a. Influence of inertia on liquid absorption into paper coating structures. Nord. Pulp Pap. Res. J. 15, 422–430.

Schoelkopf, J., Ridgway, C.J., Gane, P.A.C., Matthews, G.P., Spielmann, D.C., 2000b. Measurement and network modeling of liquid permeation into compacted mineral blocks. J. Colloid Interface Sci. 227, 119–131.

Sousa, J., Sousa, A., Podczeck, F., Newton, J.M., 1996. Influence of process conditions on drug release from pellets. Int. J. Pharm. 144, 159–169.

Vervaet, C., Baert, L., Remon, J.P., 1995. Estrusion–spheronisation—a literature review. Int. J. Pharm. 116 (1995), 131–146.

Wood, J., Gladden, L.F., 2002a. Modelling diffusion and reaction accompanied by capillary condensation using three-dimensional pore networks. Part 1. Fickian diffusion and pseudo-first-order reaction kinetics. Chem. Eng. Sci. 57, 3033–3045.

Wood, J., Gladden, L.F., 2002b. Modelling diffusion and reaction accompanied by capillary condensation using three-dimensional pore networks. Part 2. Dusty gas model and general reaction kinetics. Chem. Eng. Sci. 57, 3047–3059.

Zalc, J.M., Reyes, S.C., Iglesia, E., 2003. Monte-Carlo simulations of surface and gas phase diffusion in complex porous structures. Chem. Eng. Sci. 58, 4605–4617.

Zalc, J.M., Reyes, S.C., Iglesia, E., 2004. The effects of diffusion mechanism and void structure on transport rates and tortuosity factors in complex porous structures. Chem. Eng. Sci. 59, 2947–2960.